



HAL
open science

Luminescent and sustainable d10 coinage metal thiolate coordination polymers for high-temperature optical sensing

Ahmad Abdallah, Shefali Vaidya, Saly Hawila, Sophie-Laure Ornis, Grégoire Nebois, Adrien Barnet, Nathalie Guillou, Alexandra Fateeva, Adel Mesbah, Gilles Ledoux, et al.

► **To cite this version:**

Ahmad Abdallah, Shefali Vaidya, Saly Hawila, Sophie-Laure Ornis, Grégoire Nebois, et al.. Luminescent and sustainable d10 coinage metal thiolate coordination polymers for high-temperature optical sensing. *iScience*, 2023, 26 (2), pp.106016. 10.1016/j.isci.2023.106016 . hal-03973769

HAL Id: hal-03973769

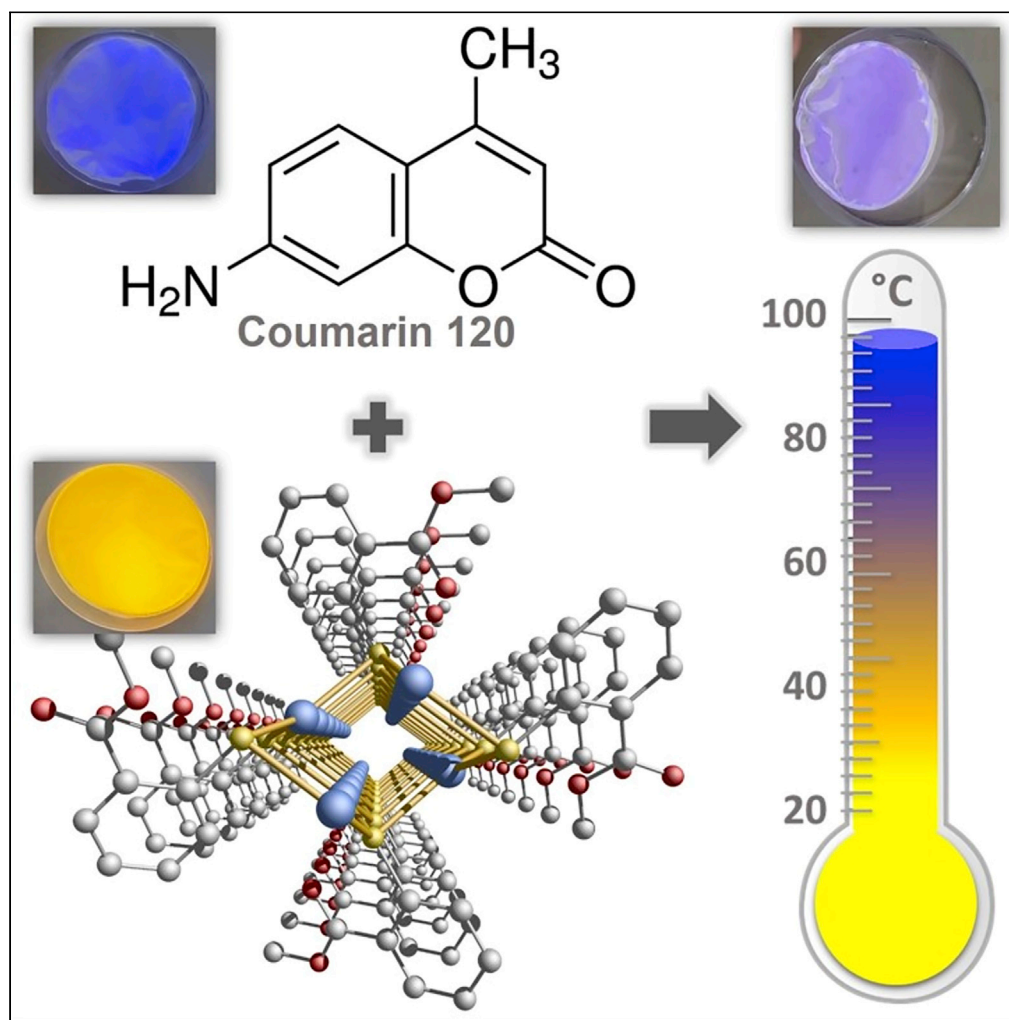
<https://hal.science/hal-03973769>

Submitted on 6 Jun 2023

HAL is a multi-disciplinary open access archive for the deposit and dissemination of scientific research documents, whether they are published or not. The documents may come from teaching and research institutions in France or abroad, or from public or private research centers.

L'archive ouverte pluridisciplinaire **HAL**, est destinée au dépôt et à la diffusion de documents scientifiques de niveau recherche, publiés ou non, émanant des établissements d'enseignement et de recherche français ou étrangers, des laboratoires publics ou privés.

Article

Luminescent and sustainable d^{10} coinage metal thiolate coordination polymers for high-temperature optical sensing

Ahmad Abdallah,
Shefali Vaidya,
Saly Hawila, ...,
Antoine Bérut,
Loïc Vanel, Aude
Demessence

aude.demessence@ircelyon.
univ-lyon1.fr

Highlights

Three 1D coordination
polymers (CP) made of d^{10}
coinage metals and
thiolate ligands

Films of PVDF polymer
with yellow-emissive silver
CP and blue-emissive
coumarin

Dual-emissive films for
ratiometric thermometry
up to 120°C

Abdallah et al., iScience 26,
106016
February 17, 2023 © 2023 The
Authors.
[https://doi.org/10.1016/
j.isci.2023.106016](https://doi.org/10.1016/j.isci.2023.106016)

Article

Luminescent and sustainable d¹⁰ coinage metal thiolate coordination polymers for high-temperature optical sensing

Ahmad Abdallah,¹ Shefali Vaidya,^{1,2} Saly Hawila,¹ Sophie-Laure Ornis,^{1,3} Grégoire Nebois,^{1,3} Adrien Barnet,^{1,3} Nathalie Guillou,⁴ Alexandra Fateeva,⁵ Adel Mesbah,¹ Gilles Ledoux,³ Antoine Bérut,³ Loïc Vanel,³ and Aude Demessence^{1,6,*}

SUMMARY

The d¹⁰ coinage metal coordination polymers (CPs) are known to display photo-physical properties which can be tuned depending on the functionality of the ligand. Three new CPs made of d¹⁰ coinage metals and methyl thiosalicylate, [M(o-SPhCO₂Me)]_n (M = Cu, Ag, Au), are reported. They are all constructed from one-dimensional metal-sulfur networks, in which Cu and Ag are three-coordinated to sulfur atoms, whereas Au is only two-coordinated. It results that both Cu(I) and Ag(I) CPs show orange photoemission at room temperature, and the Au(I) one exhibits near-infrared emission at low temperatures. The intense orange-emissive Ag(I) CP and the blue-emissive coumarin 120 have been mixed in an organic matrix, the polyvinylidene fluoride (PVDF), to form a dual luminescent flexible composite film. This film, evaluated for thermometry, shows great sensitivity for temperatures up to 100°C, a temperature never reached with non-lanthanide-based CPs.

INTRODUCTION

d¹⁰ coinage metal-based materials (Cu, Ag, Au) are known for their intense and tunable photoemission.^{1–3} Considering their sustainability and natural availability, they offer a great alternative to the conventional phosphors made of lanthanides, iridium, platinum metals, cadmium-based quantum dots, or lead halide perovskites.⁴ Luminescent composite films incorporating d¹⁰ coinage metal-based phosphors have been shown to have applications as sensors,⁵ solar concentrators, and light-emitting diodes⁶ with biocompatibility.⁷ One field of applications of luminescent materials is also the development of noninvasive thermometers having high nano- or micrometric spatial resolution and fast response.⁸ Ratiometric luminescent thermometry is based on the variation of the relative intensities of two different emission bands with temperature. These advantages of luminescent thermometers make them beneficial for many technological applications like microelectronics, microfluidics, and nanomedicine.^{9,10}

Recently, two room temperature (RT) dual-emissive films made of d¹⁰ coinage metals have been prepared by incorporating a gold-thiolate coordination polymer (CP)¹¹ and copper clusters¹² in blue-emissive organic polymers polyvinylcarbazole (PVK) and polyurethane, respectively. Moreover, thermoluminescence from RT to low temperature has also been shown with a copper-thiolate CP having intrinsic dual emission¹³ and embedded in a polyvinylidene fluoride (PVDF) matrix.¹⁴ Although, these examples show dual-emissive films working at RT or below, ratiometric films for temperature reading at RT or higher could not be obtained, due to the stability issue of the composites and/or the luminescence efficiency of the dyes. Thus, there is a tremendous need to develop efficient and sustainable temperature-sensitive films working in biological media or in everyday-life requirements, i.e., from RT up to 100°C.

Here we report the synthesis and the structural and photophysical characterizations of a new series of CPs made of d¹⁰ coinage metals and the methyl thiosalicylate [M(o-SPhCO₂Me)]_n with M = Cu (1), Ag (2), and Au (3). Films of the most emissive CP in the series, 2, have been prepared with the intense blue-emissive coumarin 120 (C) in the PVDF organic polymer, which is known for its mechanical strength and thermal and chemical stabilities. The dual-emissive film exhibits great efficiency for optical temperature reading in the RT–100°C domain.

¹Université Lyon, Université Claude Bernard Lyon 1, Institut de Recherches sur la Catalyse et l'Environnement de Lyon (IRCELYON), UMR CNRS 5256, Villeurbanne, France

²Institute of Experimental and Applied Physics, Czech Technical University in Prague, Prague, Czech Republic

³Université Lyon, Université Claude Bernard Lyon 1, Institut Lumière Matière (ILM), UMR CNRS 5306, Villeurbanne, France

⁴Université Paris-Saclay, UVSQ, Institut Lavoisier de Versailles (ILV), UMR CNRS 8180, Versailles, France

⁵Université Lyon, Université Claude Bernard Lyon 1, Laboratoire des Multimatériaux et Interfaces (LMI), UMR CNRS 5615, Villeurbanne, France

⁶Lead contact

*Correspondence: aude.demessence@ircelyon.univ-lyon1.fr

<https://doi.org/10.1016/j.isci.2023.106016>



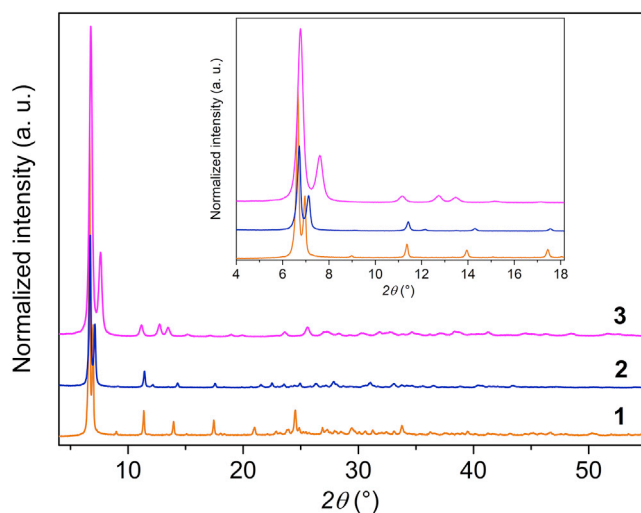


Figure 1. Powder X-ray diffraction patterns of **1**, **2**, and **3** with a zoom in the inset

RESULTS AND DISCUSSION

The $[M(o\text{-SPhCO}_2\text{Me})]_n$ ($M = \text{Cu, Ag, Au}$) CPs

Syntheses of the three $[M(o\text{-SPhCO}_2\text{Me})]_n$ CPs, **1–3**, were carried out under solvothermal conditions at 120°C, in presence of the commercially available 2-methoxythiophenol (methyl thiosalicylate) molecule, *o*-HSPHC O₂Me, by using CuCl₂·2H₂O, AgNO₃, and HAuCl₄·3H₂O, respectively. The solids were obtained with excellent yields (>76%) (see [method details](#)). The powder X-ray diffraction (PXRD) patterns of **1** and **2** ([Figure 1](#)) show that they are highly crystalline and isostructural, while **3** presents broader peaks, with slight differences in their positions. Scanning electron microscope (SEM) images ([Figure 2](#)) reveal that **1** and **2** have needle-shaped crystallites of few hundred nanometers diameter and micrometer length, while **3** is made of curved, thin, and long fibers similar to the 1D $[\text{Au}(\text{SPh})]_n$ CP.¹⁵ Their crystallographic structures were solved from PXRD data (laboratory data for **1** and synchrotron data from CRISTAL beamline of the SOLEIL facilities for **2** and **3**) (See [characterization techniques](#) for details and [Table S1](#) for crystallographic data of **1–3**, and [Figures S1–S3](#) for final Rietveld plots in [supplemental information](#)). As for the $[M(o\text{-SPhCO}_2\text{H})]_n$ ($M = \text{Cu, Ag, Au}$) series,¹⁶ the structure of **1** and **2** are 1D with ribbons made of deformed and packed M₃S₃ hexagons, whereas **3** is constructed from doubly interpenetrated helical Au-S-Au chains ([Figures 3](#) and [S4](#), representations of the structures of **2** in [supplemental information](#)). Thus, in **1** and **2**, the Cu and Ag atoms are coordinated to three sulfur atoms with S-M-S angles ranging from 115.41(2) to 121.96(2)° in **1** and from 102.70(2) to 134.44(2)° in **2** ([Table S2](#) for selected bonds and angles of **1–3** in [supplemental information](#)). In **3**, the Au atoms have their common close linear coordination mode with two sulfur atoms, and the S-Au-S angle is of 141°. The shortest metal-metal distances (excluding the metals bridged by a thiolate) are 3.506(3), 3.472(2), and 3.60(5) Å, for **1** to **3** respectively, which are at the limit to be considered as metallophilic interactions (3.5 Å) ([Figure S5](#) for representation of the Au-S chains in **3** in [supplemental information](#)).¹⁷ One particularity is the short Cu-O distances of 2.317(9) Å in **1**, between the oxygen atoms of the carbonyl groups of the ester and the metal ion. This weak interaction may participate in the self-assembly and the stabilization of the network. The infrared spectra of the compounds show the disappearance of the thiol functions at 2500 cm⁻¹, pointing out the presence of thiolate moiety coordinated to the metal ions. The antisymmetric vibration of the carbonyl function of the ester can be observed at 1700 cm⁻¹ ([Figure S6](#) for Fourier transform infrared spectroscopy [FTIR] spectra in [supplemental information](#)).¹⁶ The elemental analyses and the quantity of residues obtained after thermo-gravimetric analyses (TGA) under air of the three CPs correspond to the 1:1 metal:thiolate ligand ratio (see [method details](#) and [Figure S7](#) for TGA curves in [supplemental information](#)). In addition, TGA curves show that the compounds are stable up to 200°C under air, and PXRD patterns of the CPs heated at 150°C under air for 1 h confirm that their crystallinity is maintained ([Figure S8](#) for PXRD patterns of the heated CPs in [supplemental information](#)).

From UV-visible absorbance spectra, **1** has a band centered at 500 nm, **2** at 414 nm, and **3** at 320 nm ([Figure S9](#) for UV-visible absorption spectra in [supplemental information](#)). This gradual blue shift of the light

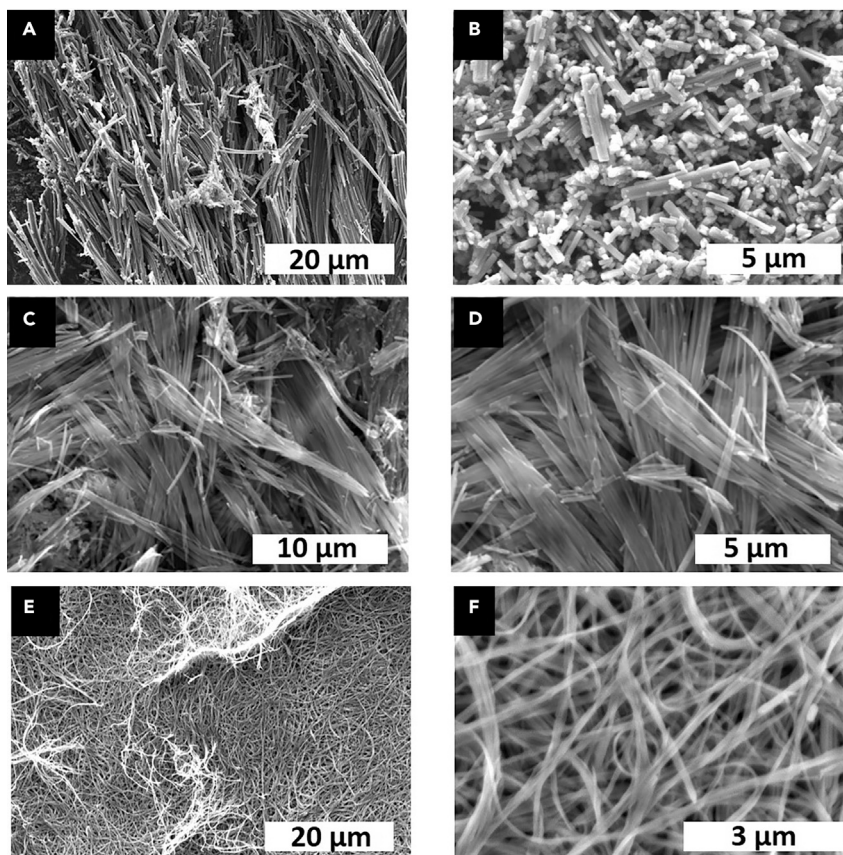


Figure 2. Scanning electron microscopy images
SEM images of 1 (A and B), 2 (C and D), and 3 (E and F).

absorption is in good agreement with the orange (1), yellow (2), and white (3) color of the CPs under natural light (Figures 4A–4C). The evaluation of the optical band gaps is around 2.17, 2.51, and 2.90 eV for 1 to 3, respectively. These values fall in the same range as those measured for the analogous $[M(o\text{-SPhCO}_2\text{H})]_n$ CPs ($M = \text{Cu}$: 2.43 eV, Ag : 2.23 eV, and Au : 2.83 eV).¹⁶

Under UV light at RT, 1 and 2 exhibit intense orange and yellow photoemission, respectively, while 3 has a very faint red color (Figures 4A–4C). From excitation/emission experiments in the solid state, at RT for 1 and 2 and at -180°C for 3, the three compounds have large single bands of excitation centered at 415 nm for 1 and 2 and at 350 nm for 3 and an emission band at 596, 600, and 820 nm, for 1 to 3, respectively (Figures 4D and S10 for emission and excitation spectra in supplemental information). Compared to the $[M(o\text{-SPhCO}_2\text{H})]_n$ ($M = \text{Cu}$, Ag , Au) series, that has its emission maxima centered at 700, 634, and 787 nm, respectively, the photoemission of 1 and 2 is blue shifted and that of 3 is red shifted to the near-infrared domain. The large Stokes shifts of 7317 and 7429 cm^{-1} for 1 and 2 at 30°C and of 16,376 cm^{-1} for 3 at -180°C , are usual for these d^{10} coinage metal CPs and are originating from phosphorescence processes.¹⁸ In addition, 1 and 2 have a quantum yield (QY) of 5 and 18%, respectively, at RT in solid state. More importantly, both yellow-emissive compounds (1 and 2) are emissive at high temperature, up to 180°C , and their decrease of the emission intensity maxima centered at 600 nm follows a quasi-linear curve for 1 and an exponential one for 2 (Figures 4E and S11–S14 for temperature-dependent excitation and emission spectra in supplemental information). Because 2 exhibits the highest QY in the series, it was selected to be embedded in PVDF-based films.

The composite films

Composite films of PVDF, 2, and/or C¹⁹ were obtained by solubilizing the PVDF in dimethylformamide (DMF) with the appropriated x and y weight percent (wt %) of the luminescent compounds to target a dual emissive film: 2_xC_y@PVDF. Then, the solution of PVDF and C, with dispersed 2 CP, is poured in a Petri dish of 9.4 cm

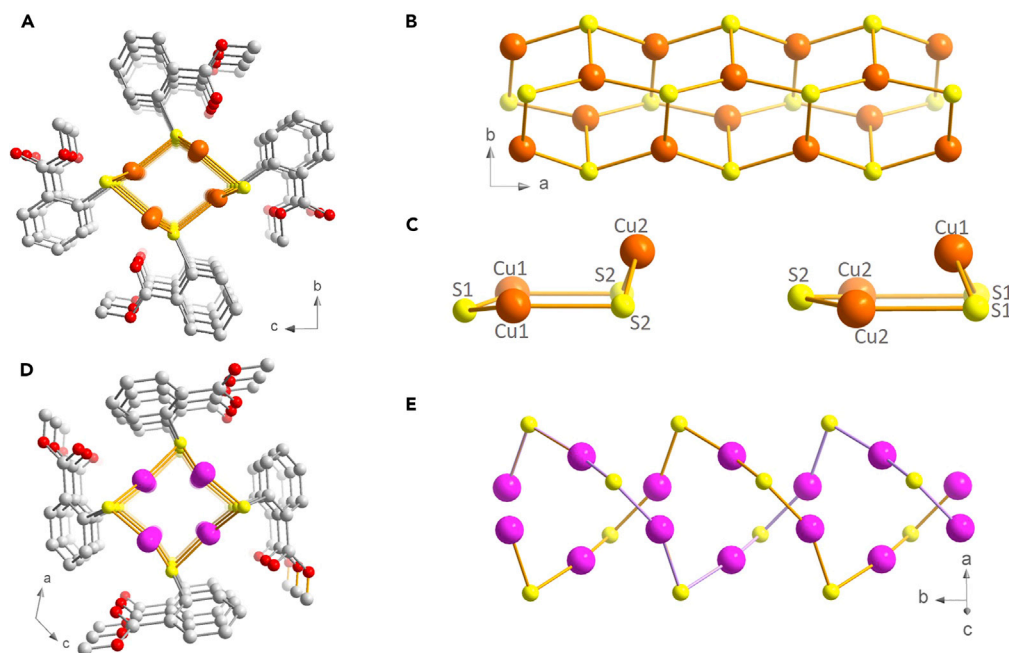


Figure 3. Crystallographic structures

Structures of **1** (A–C) and **3** (D and E): (A) projection of the helix along *a*, (B) projection along *c* of the Cu-S chain, and (C) views of the two deformed Cu₃S₃ hexagons; (D) projection of the helix along *b*, (E) Au-S chain along *b*. Orange, pink, yellow, and gray spheres correspond to copper, gold, sulfur, and carbon atoms, respectively. Hydrogen atoms were omitted for clarity.

diameter and heated between 60 and 75°C to totally evaporate the DMF solvent. Once dried, the composite films can be removed, handled, and studied. The photos of the four films of **2**@PVDF, **2**_{2.5}C_{2.5}@PVDF, **2**_{0.2}C_{0.8}@PVDF, and C@PVDF show under natural light that they are homogeneous and that the presence of **2** induces a yellow color while C@PVDF is colorless (Figure 5). The SEM images of **2**_{2.5}C_{2.5}@PVDF and **2**_{0.2}C_{0.8}@PVDF films display the surface of PVDF with some crystals of **2** (Figures S15 and S16 for SEM images in supplemental information). Under UV light, the pure films of **2**@PVDF and C@PVDF exhibit their respective intense yellow and blue photoluminescence (Figure 5) with a maximum of emission centered at 585 nm and 435 nm, respectively, at RT (Figure S17 for emission spectra of pure C@PVDF and **2**@PVDF films in supplemental information).²⁰ When **2** and C are mixed together in PVDF in a 1:1 wt % ratio, **2**_{2.5}C_{2.5}@PVDF, the film appears

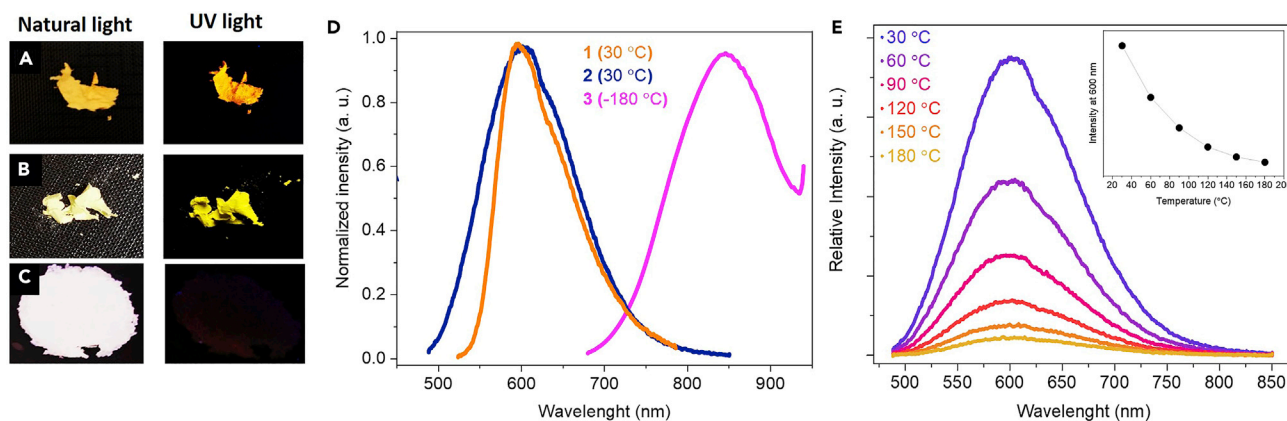


Figure 4. Photoluminescent properties

From (A) to (C): photos of **1** to **3** under natural light (left) and UV light (right) at room temperature. (D) Emission spectra ($\lambda_{\text{ex}} = 375$ nm) of **1** (orange), **2** (blue), and **3** (pink) carried out in solid state at 30°C for **1** and **2** and at –180°C for **3**. (E) Emission spectra ($\lambda_{\text{ex}} = 375$ nm) of **2** carried out in solid state from 30°C to 180°C, inset the evolution of the intensity at 600 nm with temperature.

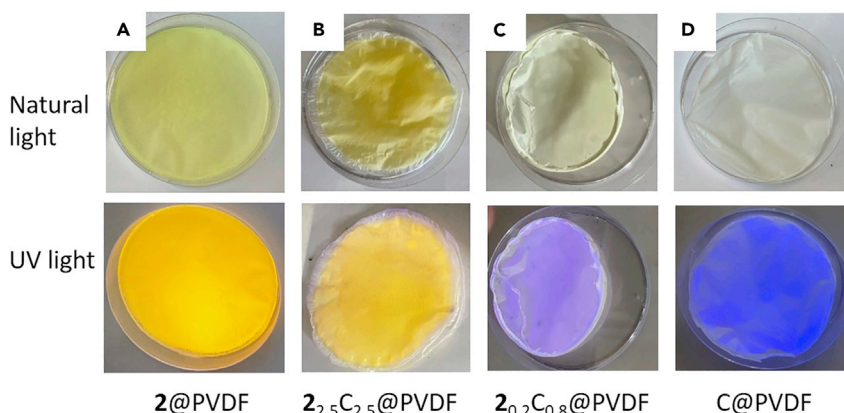


Figure 5. Composite samples

Photos at RT of the composite films under natural and UV lights: (A) 2@PVDF, (B) 2_{2.5}C_{2.5}@PVDF, (C) 2_{0.2}C_{0.8}@PVDF, and (D) C@PVDF.

yellow emissive and the emission spectrum at RT displays a weak blue band and an almost ten times more intense yellow band (Figures 5 and S18 for emission spectrum of 2_{2.5}C_{2.5}@PVDF in supplemental information). This large difference between the intensities of the two bands is not appropriate for ratiometric temperature reading. Thus, the 2_{0.2}C_{0.8}@PVDF composite film, obtained from a 4 to 1 wt % ratio of C to the CP is more appropriated. Indeed, under UV light, it exhibits a light blue color (Figure 5), and the emission spectrum shows a blue band centered at 450 and a yellow one at 610 nm with I_{450}/I_{610} ratio of 1.9 (Figure 6A). Upon increasing the temperature, the emission of 2 drops gradually, as observed before, but the intensity of the C remains almost constant (Figures 6A and 6B).²¹ Thus, the C can be considered as a reference, and the I_{450}/I_{610} intensities ratio can be plotted and fitted with an empirical Boltzmann sigmoidal function curve from 20 to 120°C, demonstrating the efficiency of the composite film as temperature sensor (Figures 6C and S19 for evolution with the temperature of the I_{450}/I_{610} ratio in supplemental information). The relative sensitivity (S_r), which allows to evaluate the performances of different ratiometric thermometers,¹¹ reaches a maximum of 2.4%.K⁻¹ at 69°C (Figure 6C). To the best of our knowledge, this sensitivity is the first one reported at such a high temperature among the CP-based materials avoiding lanthanides.²² Hence, this coumarin/CP embedded in PVDF matrix turns out to be a good dual-emissive material as luminescent temperature sensing working up to 120°C.

Mechanical properties

Evaluation of the mechanical properties of the composite 2_{0.2}C_{0.8}@PVDF film has been carried out and compared to the pure film of PVDF prepared in similar conditions (Table 1). The stress-strain curves of

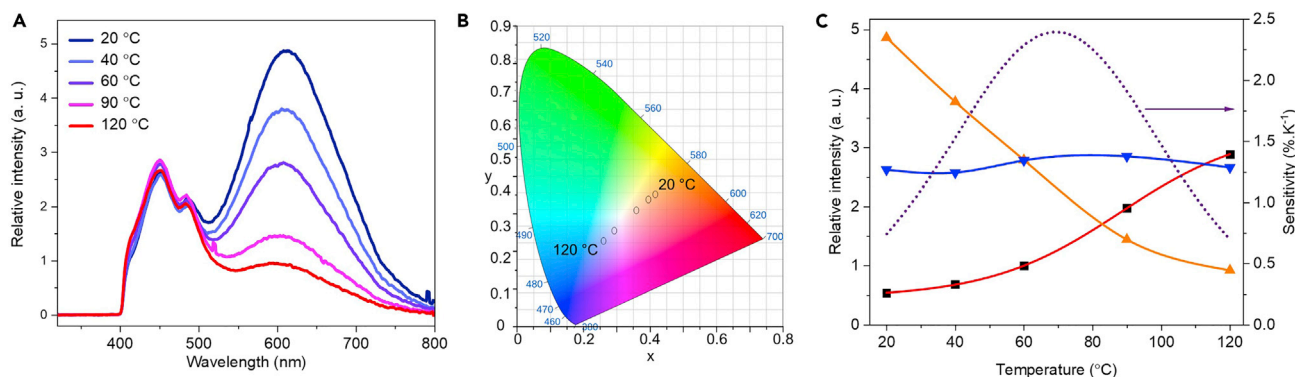


Figure 6. Luminescent properties with temperature of the composite film

(A) Photoemission ($\lambda_{ex} = 300$ nm) of 2_{0.2}C_{0.8}@PVDF film with temperature from 20 to 120°C, (B) the corresponding CIE (Commission Internationale de l'Eclairage) chromaticity diagram showing the temperature-dependence luminescence color and (C) the evolution with the temperature of the emission intensities centered at 450 nm (blue triangles), 610 nm (orange triangles), and the I_{450}/I_{610} ratio (black squares) with its Boltzmann fit (red curve) and the relative sensitivity (S_r , purple dotted curve).

Table 1. Mechanical properties of films of pure PVDF (8 samples average) and $2_{0.2}C_{0.8}@PVDF$ (5 samples average)

Sample	Young modulus (MPa)	Ultimate tensile stress (MPa)	Elongation at break (%)
Pure PVDF	320 ± 53	42.0 ± 3.5	141 ± 28
$2_{0.2}C_{0.8}@PVDF$	229 ± 61	45.6 ± 4.9	149 ± 35

two different pieces of cut films show a rather high heterogeneity of the samples (Figure 7). However, no significant difference was observed between films of pure PVDF and composite film of $2_{0.2}C_{0.8}@PVDF$.

Overall, the $2_{0.2}C_{0.8}@PVDF$ composite film presents both good elasticity and resistance, and a rather high plastic deformation domain, with values similar to the ones measured and known for films of PVDF obtained from different processes.^{23–27} Therefore, addition of CP crystallites and coumarin 120 molecules does not disturb the intrinsic mechanical properties of the PVDF and allows us to device flexible dual-emissive films.⁷

Conclusions

Three new CPs made of d^{10} coinage metals and methyl thiosalicylate ligands have been synthesized, and their crystallographic structures have been solved from PXRD. They all present 1D structures, built from M_3S_3 hexagons packed in tubular chains in the case of copper- and silver-based CPs, and built from two interpenetrating helical Au-S-Au chains for gold CP. In terms of photophysical properties, the copper- and silver-based CPs exhibit orange-yellow photoemission at RT and the gold CP has a near-infrared emission at low temperature. Owing to its intense yellow emission from RT to 180°C, $[Ag(o-SPhC O_2Me)]_n$ has been mixed with the blue-emissive coumarin 120 in the PVDF organic polymer to get a composite film exhibiting dual emission. More importantly, the intensities ratio of these two emission bands follows a Boltzmann curve from RT to 120°C making this film a good temperature sensor. This work shows that the use of sustainable, highly stable, and bright-emissive d^{10} coinage metal-thiolate-based CPs allow to target high-temperature reading, opening the path to daily-life applications.

Limitations of the study

The study has been done on few hundred milligrams scale.

STAR★METHODS

Detailed methods are provided in the online version of this paper and include the following:

- KEY RESOURCES TABLE
- RESOURCE AVAILABILITY
 - Lead contact
- METHOD DETAILS
 - Syntheses of the coordination polymers
 - Fabrication of the composite films
 - Characterization techniques

SUPPLEMENTAL INFORMATION

Supplemental information can be found online at <https://doi.org/10.1016/j.isci.2023.106016>.

ACKNOWLEDGMENTS

The authors acknowledge SOLEIL synchrotron (Gif-sur-Yvette, France) for provision of radiation facilities (BAG for X-ray diffraction 20201440) and Erik Elkaïm for assistance in using CRISTAL beamline. The authors acknowledge the CTμ for providing the SEM. This work was supported by the CNRS and its Mission for Transversal and Interdisciplinary Initiatives and by the LABEX iMUST of the University of Lyon (ANR-10-LABX-0064), created within the « Plan France 2030 » set up by the French government and managed by the French National Research Agency (ANR). AA acknowledges the Fondation de la Maison de la Chimie for his postdoctoral position, and SH, the CNRS for her PhD grant. The European Commission is acknowledged by AD for her Marie Skłodowska-Curie Individual Fellowship (101031503 — AniMOC — H2020-MSCA-IF-2020).

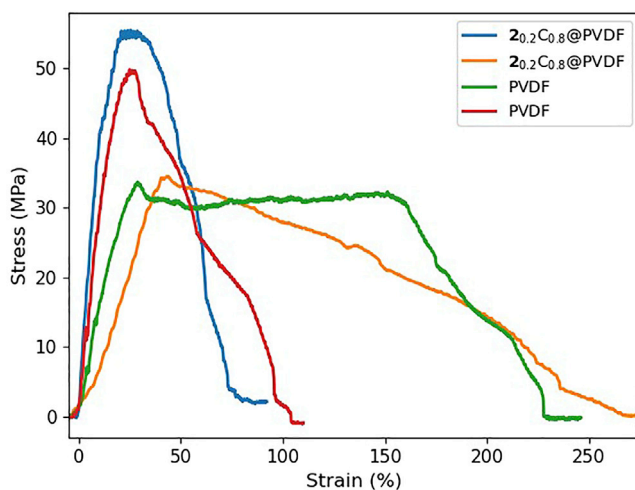


Figure 7. Typical stress-strain curves obtained for pure PVDF samples (red, green) and composite samples (blue, orange)

Results show an intrinsic heterogeneity of each film but no significant influence of the crystallites and coumarin molecules on the mechanical properties of the films.

AUTHOR CONTRIBUTIONS

AA and SV performed the synthetic experiments and routine characterizations of the CPs. SH, SLO, GN, and ABa carried out the fabrication of the composite films and their characterizations. AF performed the SEM images. NG and AM solved the structures. GL carried out the photoluminescent experiments. ABé performed the mechanical characterizations. AD, ABé, and LV conceptualized the project and supervised. AD wrote the manuscript.

DECLARATION OF INTERESTS

There are no conflicts to declare.

INCLUSION AND DIVERSITY

We support inclusive, diverse, and equitable conduct of research.

Received: October 14, 2022

Revised: December 20, 2022

Accepted: January 14, 2023

Published: February 17, 2023

REFERENCES

1. Yam, V.W.-W., Au, V.K.-M., and Leung, S.Y.-L. (2015). Light-emitting self-assembled materials based on d^9 and d^{10} transition metal complexes. *Chem. Rev.* 115, 7589–7728. <https://doi.org/10.1021/acs.chemrev.5b00074>.
2. Czerwieńiec, R., Leitzl, M.J., Homeier, H.H., and Yersin, H. (2016). Cu(I) complexes – thermally activated delayed fluorescence. Photophysical approach and material design. *Coord. Chem. Rev.* 325, 2–28. <https://doi.org/10.1016/j.ccr.2016.06.016>.
3. Yang, T.Q., Peng, B., Shan, B.Q., Zong, Y.X., Jiang, J.G., Wu, P., and Zhang, K. (2020). Origin of the photoluminescence of metal nanoclusters: from metal-centered emission to ligand-centered emission. *Nanomaterials* 10, 261. <https://doi.org/10.3390/nano10020261>.
4. (2017). Report on Critical Raw Materials for the EU. <https://ec.europa.eu/growth/sectors/raw-materials/specific-interest/critical>.
5. Conesa-Egea, J., Nogal, N., Martínez, J.I., Fernández-Moreira, V., Rodríguez-Mendoza, U.R., González-Platas, J., Gómez-García, C.J., Delgado, S., Zamora, F., and Amo-Ochoa, P. (2018). Smart composite films of nanometric thickness based on copper-iodine coordination polymers. *Chem. Sci.* 9, 8000–8010. <https://doi.org/10.1039/C8SC03085E>.
6. Wang, Z., Xiong, Y., Kershaw, S.V., Chen, B., Yang, X., Goswami, N., Lai, W.-F., Xie, J., and Rogach, A.L. (2017). In situ fabrication of flexible, thermally stable, large-area, strongly luminescent copper nanocluster/polymer composite films. *Chem. Mater.* 29, 10206–10211. <https://doi.org/10.1021/acs.chemmater.7b04239>.
7. Conesa-Egea, J., Moreno-Vázquez, A., Fernández-Moreira, V., Ballesteros, Y., Castellanos, M., Zamora, F., and Amo-Ochoa, P. (2019). Micro and nano smart composite films based on copper-iodine coordination polymer as thermochromic biocompatible sensors. *Polymers* 11, 1047. <https://doi.org/10.3390/polym11061047>.
8. Jaque, D., and Vetrone, F. (2012). Luminescence nanothermometry. *Nanoscale* 4, 4301–4326. <https://doi.org/10.1039/C2NR30764B>.

9. Uchiyama, S., and Gota, C. (2017). Luminescent molecular thermometers for the ratiometric sensing of intracellular temperature. *Rev. Anal. Chem.* 36. <https://doi.org/10.1515/revac-2016-0021>.
10. Xu, M., Zou, X., Su, Q., Yuan, W., Cao, C., Wang, Q., Zhu, X., Feng, W., and Li, F. (2018). Ratiometric nanothermometer in vivo based on triplet sensitized upconversion. *Nat. Commun.* 9, 2698. <https://doi.org/10.1038/s41467-018-05160-1>.
11. Veselska, O., Guillou, N., Ledoux, G., Huang, C.-C., Dohnalova Newell, K., Elkaim, E., Fateeva, A., and Demessence, A. (2019). A new lamellar gold thiolate coordination polymer, [Au(m-SPhCO₂H)]_n, for the formation of luminescent polymer composites. *Nanomaterials* 9, 1408. <https://doi.org/10.3390/nano9101408>.
12. Wang, Z., Chen, B., Zhu, M., Kershaw, S.V., Zhi, C., Zhong, H., and Rogach, A.L. (2016). Stretchable and thermally stable dual emission composite films of on-purpose aggregated copper nanoclusters in carboxylated polyurethane for remote white light-emitting devices. *ACS Appl. Mater. Interfaces* 8, 33993–33998. <https://doi.org/10.1021/acsami.6b10828>.
13. Veselska, O., Podbevšek, D., Ledoux, G., Fateeva, A., and Demessence, A. (2017). Intrinsic triple-emitting 2D copper thiolate coordination polymer as a ratiometric thermometer working over 400 K range. *Chem. Commun.* 53, 12225–12228. <https://doi.org/10.1039/C7CC06815H>.
14. Troyano, J., Castillo, O., Martínez, J.I., Fernández-Moreira, V., Ballesteros, Y., Maspocho, D., Zamora, F., and Delgado, S. (2018). Reversible thermochromic polymeric thin films made of ultrathin 2D crystals of coordination polymers based on copper(I)-Thiophenolates. *Adv. Funct. Mater.* 28, 1704040. <https://doi.org/10.1002/adfm.201704040>.
15. Vaidya, S., Veselska, O., Zhadan, A., Daniel, M., Ledoux, G., Fateeva, A., Tsuruoka, T., and Demessence, A. (2020). Flexible and luminescent fibers of a 1D Au(I)-thiophenolate coordination polymer and formation of gold nanoparticle-based composite materials for SERS. *J. Mater. Chem. C* 8, 8018–8027. <https://doi.org/10.1039/D0TC01706J>.
16. Veselska, O., Guillou, N., Diaz-Lopez, M., Bordet, P., Ledoux, G., Lebègue, S., Mesbah, A., Fateeva, A., and Demessence, A. (2022). Sustainable and efficient low-energy light emitters: a series of one-dimensional d¹⁰ coinage metal-organic chalcogenolates, [M(o-SPhCO₂H)]_n. *ChemPhotoChem* 6, e202200030. <https://doi.org/10.1002/cptc.202200030>.
17. Veselska, O., and Demessence, A. (2018). d¹⁰ coinage metal organic chalcogenolates: from oligomers to coordination polymers. *Coord. Chem. Rev.* 355, 240–270. <https://doi.org/10.1016/j.ccr.2017.08.014>.
18. Sun, P., Xie, M., Zhang, L.-M., Liu, J.-X., Wu, J., Li, D.-S., Yuan, S.-F., Wu, T., and Li, D. (2022). Ultrastable anti-acid “shield” in layered silver coordination polymers. *Angew. Chem., Int. Ed. Engl.* 61, e202209971. <https://doi.org/10.1002/anie.202209971>.
19. Wagner, B.D. (2009). The use of coumarins as environmentally-sensitive fluorescent probes of heterogeneous inclusion systems. *Molecules* 14, 210–237. <https://doi.org/10.3390/molecules14010210>.
20. Park, S.-Y., Ebihara, M., Kubota, Y., Funabiki, K., and Matsui, M. (2009). The relationship between solid-state fluorescence intensity and molecular packing of coumarin dyes. *Dyes Pigments* 82, 258–267. <https://doi.org/10.1016/j.dyepig.2009.01.014>.
21. Dobek, K., and Karolczak, J. (2012). The influence of temperature on C153 steady-state absorption and fluorescence kinetics in hydrogen bonding solvents. *J. Fluoresc.* 22, 1647–1657. <https://doi.org/10.1007/s10895-012-1109-2>.
22. Yang, Y., Chen, L., Jiang, F., Yu, M., Wan, X., Zhang, B., and Hong, M. (2017). A family of doped lanthanide metal-organic frameworks for wide-range temperature sensing and tunable white light emission. *J. Mater. Chem. C* 5, 1981–1989. <https://doi.org/10.1039/C6TC05316E>.
23. Liu, Y., Sun, Y., Zeng, F., Chen, Y., Li, Q., Yu, B., and Liu, W. (2013). Morphology, crystallization, thermal, and mechanical properties of poly(vinylidene fluoride) films filled with different concentrations of polyhedral oligomeric silsesquioxane. *Polym. Eng. Sci.* 53, 1364–1373. <https://doi.org/10.1002/pen.23398>.
24. Zeng, F., Liu, Y., Sun, Y., Hu, E., and Zhou, Y. (2012). Nanoindentation, nanoscratch, and nanotensile testing of poly(vinylidene fluoride)-polyhedral oligomeric silsesquioxane nanocomposites. *J. Polym. Sci. B Polym. Phys.* 50, 1597–1611. <https://doi.org/10.1002/polb.23159>.
25. Yun, J.S., Park, C.K., Jeong, Y.H., Cho, J.H., Paik, J.-H., Yoon, S.H., and Hwang, K.-R. (2016). The fabrication and characterization of piezoelectric PZT/PVDF electrospun nanofiber composites. *Nanomater. Nanotechnol.* 6, 20. <https://doi.org/10.5772/62433>.
26. Zaccaria, M., Fabiani, D., Cannucciari, G., Gualandi, C., Focarete, M.L., Arbizzani, C., De Giorgio, F., and Mastragostino, M. (2015). Effect of silica and tin oxide nanoparticles on properties of nanofibrous electrospun separators. *J. Electrochem. Soc.* 162, A915–A920. <https://doi.org/10.1149/2.0421506jes>.
27. Lu, H., and Li, L. (2018). Crystalline structure, dielectric, and mechanical properties of simultaneously biaxially stretched poly(vinylidene fluoride) film. *Polym. Adv. Technol.* 29, 3056–3064. <https://doi.org/10.1002/pat.4426>.

STAR★METHODS

KEY RESOURCES TABLE

REAGENT or RESOURCE	SOURCE	IDENTIFIER
Chemicals, peptides, and recombinant proteins		
Copper(II) chloride dihydrate	Sigma Aldrich	10125-13-0
Silver nitrate	Sigma Aldrich	7761-88-8
Gold(III) chloride trihydrate	Sigma Aldrich	16961-25-4
Poly(vinylidene fluoride) average $M_w \sim 534,000$	Sigma Aldrich	24937-79-9
7-Amino-4-methylcoumarin	Sigma Aldrich	26093-31-2
Methyl thiosalicylate	Sigma Aldrich	4892-02-8
Deposited data		
$[\text{Cu}(\text{o-SPhCO}_2\text{Me})]_n$	Cambridge Crystallographic Data Centre	CCDC-2212136
$[\text{Ag}(\text{o-SPhCO}_2\text{Me})]_n$	Cambridge Crystallographic Data Centre	CCDC-2212139
$[\text{Au}(\text{o-SPhCO}_2\text{Me})]_n$	Cambridge Crystallographic Data Centre	CCDC-2212140

RESOURCE AVAILABILITY

Lead contact

Further information and requests for resources and reagents should be directed to and will be fulfilled by the lead contact, Aude Demessence (aude.demessence@ircelyon.univ-lyon1.fr).

METHOD DETAILS

Syntheses of the coordination polymers

Synthesis of $[\text{Cu}(\text{o-SPhCO}_2\text{Me})]_n$

A solution of $\text{CuCl}_2 \cdot 2\text{H}_2\text{O}$ (63 mg, 0.37 mmol) in 4 mL of DMF, was added to a solution of *o*-HSP HCO_2Me (87 mg, 71 μL , 0.514 mmol) dissolved in 4 mL of DMF. Then followed by the addition of 2 mL of H_2SO_4 (0.5 M). The mixture was introduced into a 20 mL glass vial, sealed and heated at 120°C for 24 h. The resulting orange solid is filtered and washed three times with ethanol and three times with acetone and then dried in air. The solid is not soluble in any solvent and it shows very thick fibers unsuitable for single crystal XRD. Yield: 87 % (50.3 mg). Chemical Formula: $\text{C}_8\text{H}_7\text{CuO}_2\text{S}$. Molecular Weight: 230.75 g/mol. CuO content from TGA (calc.) wt%: 34 (34.54). Elemental analysis: exp. (calc.) %: C, 39.2 (41.2); H, 2.95 (3.06); S, 14.45 (13.9).

Synthesis of $[\text{Ag}(\text{o-SPhCO}_2\text{Me})]_n$

A solution of AgNO_3 (100 mg, 0.59 mmol) in H_2O (5 mL) was added to *o*-HSP HCO_2Me (100 mg, 81.5 μL , 0.59 mmol) dissolved in DMF (5 mL). The reaction was allowed to proceed for 24 h at 120 °C in a 20 ml sealed glass vial. A yellow precipitate was obtained and washed 3 times with 20 mL of DMF, and 3 times with 20 mL of acetone. Yield: 97 % (158.5 mg). Chemical Formula: $\text{C}_8\text{H}_7\text{AgO}_2\text{S}$. Molecular Weight: 275 g/mol. Solid Ag content from TGA (calc.) wt%: 39.5 (39.2). Elemental analysis: exp. (calc.) %: C, 34.57 (34.93); H, 2.38 (2.56); S, 12.29 (11.66).

Synthesis of $[\text{Au}(\text{o-SPhCO}_2\text{Me})]_n$

o-HSP HCO_2Me (1.3 g, 1064 μL , 10.15 mmol) was added to a solution of $\text{HAuCl}_4 \cdot 3\text{H}_2\text{O}$ (100 mg, 0.25 mmol) in EtOH (10 mL). The reaction was allowed to proceed for 18 h at 120 °C in a 20 ml sealed glass vial. A white fibrous precipitate was obtained and washed 3 times with 50 mL of EtOH. Yield: 76 % (70 mg). Chemical Formula: $\text{C}_8\text{H}_7\text{O}_2\text{SAu}$. Molecular Weight: 364 g/mol. Solid Au content from TGA (calc.) wt%: 54.8 (54.07). Elemental analysis: exp. (calc.) %: C, 25.7 (26.4); H, 1.48 (1.94); S, 9.74 (8.8); O, 8.5 (8.79).

Fabrication of the composite films

Synthesis of 2@PVDF

Powders of 423 mg of PVDF (94.2 wt%) and 26 mg (5.8 wt%) of **2** are introduced in a vial and then 12 mL of DMF are added. The mixture is sonicated for 10 min to solubilize the PVDF and dispersed the CP aggregates. Then, the solution is poured in a disposable Petri dish of 94 mm × 16 mm (L × W) and heated on a heating plate at 75 °C until the total evaporation of the DMF (around 30-45 min). Finally, the film can be easily handled.

Synthesis of C@PVDF

Powders of 415 mg of PVDF (95.1 wt%) and 22 mg (4.9 wt%) of 7-Amino-4-methylcoumarin (C120) are introduced in a vial and then 12 mL of DMF are added. The mixture is sonicated for 10 min to solubilize the PVDF and dispersed the CP aggregates. Then, the solution is poured in a disposable Petri dish of 94 mm × 16 mm (L × W) and heated on a heating plate at 75 °C until the total evaporation of the DMF (around 30-45 min). Finally, the film can be easily handled.

Synthesis of 22.5C2.5@PVDF

Powders of 400 mg of PVDF (95 wt%), 10 mg (2.5 wt%) of **2** and 10 mg (2.5 wt%) of 7-Amino-4-methylcoumarin (C120) are introduced in a vial and then 12 mL of DMF are added. The mixture is sonicated for 10 min to solubilize the PVDF and dispersed the CP aggregates. Then, the solution is poured in a disposable Petri dish of 94 mm × 16 mm (L × W) and heated on a heating plate at 60 °C until the total evaporation of the DMF (around 30-45 min). Finally, the film can be easily handled.

Synthesis of 20.2C0.8@PVDF

Powders of 400 mg of PVDF (99 wt%), 1 mg (0.2 wt%) of **2** and 3 mg (0.8 wt%) of 7-Amino-4-methylcoumarin (C120) are introduced in a vial and then 12 mL of DMF are added. The mixture is sonicated for 10 min to solubilize the PVDF and dispersed the CP aggregates. Then, the solution is poured in a disposable Petri dish of 94 mm × 16 mm (L × W) and heated on a heating plate at 60 °C until the total evaporation of the DMF (around 30-45 min). Finally, the film can be easily handled.

Characterization techniques

Routine PXRD

Routine powder X-ray diffraction was carried out on a Bruker D8 Advance A25 diffractometer using Cu K α radiation equipped with a 1-dimensional position-sensitive detector (Bruker LynxEye). XR scattering was recorded between 4° and 90° (2 θ) with 0.02° steps and 0.5 s per step (28 min for the scan). Divergence slit was fixed to 0.2° and the detector aperture to 189 channels (2.9°).

FTIR

The infrared spectra were obtained from a Bruker Vector 22 FT-IR spectrometer with KBr pellets at room temperature and registered from 4000 cm⁻¹ to 400 cm⁻¹.

TGA

Thermo-gravimetric analyses (TGA) were performed with a TGA/DSC 1 STArE System from Mettler Toledo. Around 2 mg of sample was heated at a rate of 10 °C.min⁻¹, in a 70 μ L alumina crucible, under air atmosphere (20 mL.min⁻¹).

SEM

SEM images were obtained with FEI Quanta 250 FEG scanning electron microscope. Samples were mounted on stainless pads and sputtered with carbon to prevent charging during observation.

UV-vis

UV-vis absorption spectrum was carried out with a LAMBDA 365 UV/Vis Spectrophotometer from Perkin Elmer in solid state with KBr at room temperature.

Structural determinations

High-resolution X-ray powder diffraction (HRXRPD) data of compound **1** were collected in the 4-100 (° 2 θ) range with the Debye-Scherrer geometry, on a Bruker D8 Advance diffractometer,

equipped with a Ge(111) monochromator producing Cu $K\alpha_1$ radiation ($\lambda = 1.540598 \text{ \AA}$) and a LynxEye detector.

For compounds **2** and **3**, HRXRPD data were collected on the CRISTAL beamline at SOLEIL Synchrotron (Gif-sur-Yvette, France). A monochromatic beam was extracted from the U20 undulator beam by means of a Si(111) double monochromator. Wavelengths of 0.72844 and 0.67122 \AA were refined from a LaB6 (NIST Standard Reference Material 660a) powder diagram recorded prior to the experiment for **2** and **3**, respectively. Diffraction data were collected in continuous scanning mode with a MYTHEN2 X 9K detector (Dectris) allowing measurement in less than 5 minutes.

The three samples were loaded in 0.5 (**1**) and 0.7 mm (**2** and **3**) capillaries (Borokapillaren, GLAS, Schönwalde, Germany) mounted on a spinner rotating to improve the particles' statistics.

Calculations of structural investigations (indexing, charge flipping, simulated annealing, difference Fourier calculations, Rietveld refinement) were performed with the TOPAS V5.0 software and EXPO (direct methods) program (A. Altomare et al., *J. Appl. Cryst.*, 2013, **46**, 1231). For **1** and **2**, the LSI-indexing method converged unambiguously to a monoclinic unit cell with satisfactory figures of Merit (see [Table S1 in supplemental information](#)). Systematic extinctions were consistent with the $P2_1/c$ space group. For **3**, given its poor crystallinity, indexing of its powder pattern was a bit more ambiguous, but similarities with the unit cell parameters of $[\text{Au}(\text{SPh})]_n$ (C. Lavenn et al., *J. Mater. Chem. C*, 2015, **3**, 4115) led us to choose among the proposed the unit cells, the one compatible with the $C2/c$ space group. The structure of **1** and **2** was investigated from data of the copper compound. Direct methods led us to locate unambiguously the two independent metal atoms as well as the two sulfur ones. The corresponding atomic coordinates were then used as the starting model in the Rietveld refinement, and fixed, in order to localize the organic moieties, that were treated as rigid bodies, by simulated annealing processes. The structural model of **1** was then directly used to refine the structure of **2**. For **3**, the structure of $[\text{Au}(\text{SPh})]_n$ was used as the starting model in the Rietveld refinement and the same strategy as for **1** and **2** was then used. The final Rietveld plots ([Figures S1, S2, and S3 in supplemental information](#) for **1**, **2** and **3**, respectively) correspond to satisfactory model indicators and profile factors ([Table S1 in supplemental information](#)). A small amount of 1.63(4) weight % gold has been detected on the PXRD data of **3** and has been taken into account during the Rietveld refinement. At their final stage, the Rietveld refinements involve the following structural parameters: 6 atomic coordinates, 6 translation and 6 rotation parameters for the organic molecule as well as 6 distances and 2 ester torsion angles, 1 thermal factor and 1 scale factor. CCDC-2212136, 2212139 and 2212140 contain the supplementary crystallographic data of **1**, **2** and **3**, respectively.

Photoluminescence excitation and emission spectra measurements

The photoluminescence measurements were performed on a homemade apparatus at Institut Lumière Matière, University of Lyon. The sample was illuminated by an EQ99X laser driven light source filtered by a Jobin Yvon Gemini 180 monochromator. The exit slit from the monochromator was then reimaged on the sample by two 100m focal length, 2 inch diameter MgF_2 lenses. The whole apparatus has been calibrated by means of a Newport 918D low power calibrated photodiode sensor over the range 190-1000 nm. The resolution of the system being 4 nm. The emitted light from the sample is collected by an optical fiber connected to a Jobin-Yvon TRIAX320 monochromator equipped with a cooled CCD detector. At the entrance of the monochromator different long pass filter can be chosen in order to eliminate the excitation light. The resolution of the detection system is 2 nm. Temperature control over the sample was regulated with a THMS-600 heating stage with T95-PE temperature controller from Linkam Scientific Instruments.

Mechanical experiments

Mechanical testing of the composite films was performed using a custom-made tensile test apparatus. The films have a typical thickness of about 30 to 40 μm . For each film, two to five samples of approximative dimensions 10 mm x 30 mm are manually cut and measured. Each sample is placed in an aluminium vice, and then stretched uniaxially at a constant elongation rate of 50 $\mu\text{m/s}$ thanks to a stepper motor (from Faulhaber) equipped with a reducer (from Mijno), so that each step corresponds to a displacement of 1/400 μm . The force is measured by a force transducer (from Interface) connected to an analog-to-digital acquisition card (from National Instruments). The stress-strain curves are recorded with a 1000 Hz acquisition rate, and then smoothed using a moving average to reduce electrical noise. The Young Modulus is obtained by a numerical fit of the linear part of each stress-strain curve.